R. & M. No. 3133
(19,943)
A.R.C. Technical Report

MINISTRY OF AVIATION

AERONAUTICAL RESEARCH COUNCIL
REPORTS AND MEMORANDA

Boundary-Layer Measurements on 15-deg and 24·5-deg Cones at Small Angles of Incidence at M = 3·17 and 3·82 and Zero Heat Transfer

By

F. V. DAVIES and R. J. MONAGHAN

LONDON: HER MAJESTY'S STATIONERY OFFICE
1959
PRICE 9*s*. 6*d*. NET

Boundary-Layer Measurements on 15-deg and 24·5-deg Cones at Small Angles of Incidence at M = 3·17 and 3·82 and Zero Heat Transfer

By

F. V. DAVIES and R. J. MONAGHAN

COMMUNICATED BY THE DIRECTOR-GENERAL OF SCIENTIFIC RESEARCH (AIR)
MINISTRY OF SUPPLY

Reports and Memoranda No. 3133*

June, 1957

Summary.—Transition measurements on 15-deg and 24·5-deg cones at $M_\infty = 3·17$ and 3·82 showed that the transition front was extremely sensitive to incidence, a fourfold variation occurring between transition Reynolds numbers on the leeward and windward sides of the 15-deg cone at 2-deg incidence. At zero incidence the transition Reynolds number was between 2·5 and $3·0 \times 10^6$ and no significant variation was observed over the test range of stagnation pressures from 2 to 5 atmospheres.

Pitot traverses on the top generator of the 15-deg cone at $M_\infty = 3·17$ showed that the effects of small angles of incidence (— 2 deg to + 1 deg) on the characteristics of the laminar boundary layer were nearly linear and were in excellent agreement with the theory of F. K. Moore.

The same results showed that small angles of incidence altered the thicknesses of both laminar and turbulent boundary layers, but did not affect the shapes of the velocity profiles. The alteration with incidence of the displacement thickness of the laminar boundary layer was large (agreeing with Moore's theory), and in amount was more than twice that found with a turbulent boundary layer.

Introduction.—The characteristics of laminar and turbulent boundary layers on circular cones in supersonic flow can now be predicted with reasonable accuracy for Reynolds numbers up to 10^7 and Mach numbers up to at least 5 under zero heat-transfer conditions and at zero incidence. Neither of these conditions is likely to apply at all times in practice and it is of obvious importance to determine the effects of both heat transfer and incidence on the cone boundary layer. Accordingly a test series was started and this note describes some measurements of the effects of incidence at zero heat transfer.

The effect of small angles of incidence is to perturb the axisymmetric patterns of both the inviscid flow and the boundary layer around the cone. The inviscid and viscous flows are closely interdependent; circumferential pressure gradients in the external flow inducing cross flow and consequent axial asymmetry of growth and stability in the boundary layer. The theoretical aspects are discussed in detail in Section 2.

* R.A.E. Report Aero. 2577, received 27th February, 1958.

Experimental data were obtained from tests made on two cones of 15 deg and 24·5 deg total angle in a wind tunnel of 5 in. square working-section at Mach numbers of 3·17 and 3·82 and with a stagnation pressure ranging from 2 to 5 Atm. abs. (tests involving boundary-layer traverses were made on the 15-deg cone at a Mach number of 3·17). A complete experimental investigation would require boundary-layer exploration along a number of generators. However, present test arrangements do not allow this to be done and boundary-layer traverses with a pitot-tube are confined to one generator in the plane of symmetry. Transition determinations using a chemical indicator (azo-benzene) cover the whole surface of the cone. More details are given in Section 4.

The experimental limitations are to some extent offset by the existence of a laminar-boundary-layer theory by Moore[5] which applies to the flow at all points on a cone if the incidence is small, and with which the present results are compared in Section 7.

2. *Theoretical Considerations of the General Effects of Incidence.*—The effects of incidence on a cone in supersonic flow depend upon the range of incidence considered. The range appropriate to this note is for small angles of incidence $\alpha(-2 \text{ deg} < \alpha < 2 \text{ deg})$ with a corresponding range of $\alpha/\theta(-0{\cdot}266 < \alpha/\theta < +0{\cdot}266)$ for a 15-deg cone, θ being the semi-angle* of the cone. Within these limits the cone shock remains attached and the inviscid-flow field is conical with all parameters constant along rays from the apex.

For these conditions the effects of incidence may be discussed under two headings: first the effects on the non-viscous flow external to the boundary layer and second the effects upon the boundary layer itself.

2.1. *The Effects of Incidence on the Inviscid Flow.*—The flow over a cone at zero incidence is conical in form and symmetrical about the cone axis. For small angles of incidence the apex of the conical field remains coincident with the cone tip (attached shock wave) but the axis of the field is inclined at a small angle to the cone axis in the plane of incidence. The flow parameters are constant along rays from the apex and are functions of Mach number, cone angle, incidence and the position in the flow field described by the angles θ_F and Ω as shown in Fig. 1.

The static pressure (p_1) at the surface of a cone at incidence is related to the corresponding static pressure ($\bar{p}_1$) at zero incidence by

$$\frac{p_1}{\bar{p}_1} = 1 + \alpha A_3 \cos \Omega + \alpha^2(B_3 + D_3 \cos 2\Omega) + \ldots \quad .. \quad .. \quad .. \quad (1a)$$

(α is in radians in this and similar formulae), where A_3, B_3 and D_3 are functions only of θ and M and are obtained from Ref. 2 *via* Ref. 3 (the pressure at zero incidence is constant at all points on the cone surface).

Fig. 2 shows typical theoretical pressure distributions given by equation 1 for a 15-deg (total angle) cone at incidences of 1 and 6 deg in an $M = 3{\cdot}18$ air stream. At the lower incidence there is approximately a sinusoidal variation of pressure around the circumference of the cone with higher pressure on the windward than on the leeward side. As the incidence is increased, this distribution is progressively modified by the second-order term in equation 1 until above a certain incidence (4·7 deg in the present case) a pressure minimum appears on the leeward side before the top generator ($\Omega = 180$ deg) is reached. This minimum and the subsequent adverse pressure gradient (in the circumferential direction) are illustrated by Fig. 2b for $\alpha = 6$ deg. It may be noted that adverse pressure gradients of this type should not occur within the incidence range ($-2 \text{ deg} < \alpha < +2 \text{ deg}$) of the test series of this report, either at $M = 3{\cdot}17$ or $M = 3{\cdot}82$ (at $M = 3{\cdot}82$ the critical incidence would be increased to just under 5 deg.)

* The symbol θ describing the cone semi-angle instead of total angle has been adopted to simplify the boundary-layer equations. The description of the cone models by their total angle is a continuation of the practice adopted in Refs. 7 and 9.

Other flow parameters such as density and velocity can be expressed in forms similar to that of equation (1*a*). For example, the meridional and circumferential velocities (u_1 and w_1) are given by

$$\frac{u_1}{\bar{u}_1} = 1 - \alpha A_1 \cos \Omega + \alpha^2(B_1 + D_1 \cos 2\Omega) + \ldots , \quad .. \quad .. \quad .. \quad (1b)$$

$$\frac{w_1}{\bar{u}_1} = \alpha A_2 \sin \Omega + \alpha^2 D_2 \sin 2\Omega + \ldots , \quad .. \quad .. \quad .. \quad .. \quad .. \quad (1c)$$

where, as before, the A and D are functions only of θ and M and are obtained from Ref. 2 *via* Ref. 3.

2.2. *The Effects of Incidence on the Boundary Layer.*—The circumferential pressure gradients illustrated in Fig. 2 affect both the growth and stability of the laminar boundary layer by inducing cross flows. Because the static pressure is constant across the layer, the pressure gradient is likewise constant and thus the air with low momentum near the wall will follow the direction of the gradient more closely than the air with higher momentum near the outer edge of the layer. Some practical implications of this divergence are considered in Section 4.1 in connection with the use of pitot-tubes for traversing the boundary layer.

At small positive angles of incidence (more strictly α/θ small), the circumferential pressure gradient is favourable from $\Omega = 0$ to $\Omega = 180$ deg (Fig. 2*a*) and the boundary layer is drained from the windward side to the leeward side, thinning on the windward side and thickening on the leeward side. As α/θ increases, an adverse pressure gradient appears on the leeward side (Fig. 2*b*), which eventually becomes strong enough to cause cross-flow separation with the formation of vortex lobes. However, these latter flow conditions are outside the scope of the present report.

A further effect of the draining of the boundary layer from one side of the cone to the other is that the stability of the thinned layer is increased and that of the thickened layer is decreased. It follows that the transition 'front' at which the boundary layer becomes turbulent will be distorted from that corresponding to zero incidence.

F. K. Moore has obtained some theoretical solutions[1,4,5] of the laminar boundary layer on a cone at incidence. The particular solution to be summarised here is that from a small perturbation analysis applicable to all positions on the cone for $\alpha/\theta << 1$ and *a priori* valid only in the limiting case of vanishing angle of attack. The following general assumptions were made:

(*a*) The boundary layer does not modify the external flow field, which is given by equation (1) above, neglecting terms higher than the first order in α

(*b*) Zero heat-transfer conditions exist at the cone surface

(*c*) Prandtl number $\sigma = 1$,

(*d*) The Sutherland viscosity law can be approximated to by

$$\mu/\mu_r = C(T/T_r) , \quad .. \quad .. \quad .. \quad .. \quad .. \quad .. \quad .. \quad .. \quad (2)$$

where subscript r refers to a reference condition

(*e*) The specific heats are constant, with the ratio

$$C_p/C_v = \gamma = 1{\cdot}4 .$$

The solutions are given in terms of the angle Ω defining the circumferential position on the cone (Fig. 1), incidence α and the Mach number outside the boundary layer on the cone at zero incidence $\bar{M}_1$.

2.2.1. *Velocity profiles.*—Solutions for the velocity profiles are,

$$u/u_1 = f_0' + \alpha A_1 \cos \Omega \left[\left(1 - \frac{2}{3 \sin \theta} \frac{A_2}{A_1} \right) (f_0' - h_2') - 2 \left(1 + \frac{\gamma - 1}{2} \bar{M}_1^2 \right) \frac{A_2}{A_1 \sin \theta} h_3' \right] \quad .. \quad .. \quad .. \quad .. \quad (3)$$

for the meridional profile and

$$\frac{w}{w_1} = f_0' + \left(1 + \frac{\gamma - 1}{2} \bar{M}_1^2 \right) h_1' \quad .. \quad .. \quad .. \quad .. \quad .. \quad (4)$$

for the circumferential profile.

A_1 and A_2 are the coefficients occurring in equations (1) which specify the first-order effects of incidence on the inviscid flow and are functions of cone angle and free-stream Mach number (Refs. 2 and 3).

f_0', h_1', h_2' and h_3' refer to the viscous flow in the boundary layer and are tabulated in Ref. 5 as functions of a non-dimensional co-ordinate λ_L.

This co-ordinate λ_L is the similarity parameter $Y/X^{1/2}$ of an equivalent two-dimensional incompressible boundary layer, obtained from the physical co-ordinates (x, y) by Howarth's transformation between compressible and incompressible flow

$$\left. \begin{aligned} Y' &= \left(\frac{\rho}{\bar{\rho}} \right)^{-1/2} \int_0^{y'} \frac{\rho}{\bar{\rho}_1} dy' \\ X &= x' \end{aligned} \right\}, \quad .. \quad .. \quad .. \quad .. \quad .. \quad .. \quad .. \quad (5)$$

where

$$\left. \begin{aligned} x' &= \frac{\bar{\rho}_1 \bar{u}_1}{\bar{\mu}_1} \frac{x}{C}, \\ y' &= \frac{\bar{\rho}_1 \bar{u}_1}{\bar{\mu}_1} \frac{y}{C} \end{aligned} \right\} \quad .. \quad .. \quad .. \quad .. \quad .. \quad .. \quad .. \quad (6)$$

(bars denoting zero incidence and C from equation (2) taking $T_r = T_w$ where T_w is wall temperature), and by applying Mangler's $\sqrt{3}$ transformation between conical flow and plane flow, *i.e.*,

$$Y = \sqrt{3} Y' . \quad .. \quad .. \quad .. \quad .. \quad .. \quad .. \quad .. \quad .. \quad (7)$$

Applying these transformations we have

$$\lambda_L = Y/X^{1/2} = \sqrt{3} \left\{ \left(\frac{\rho}{\bar{\rho}} \right)^{-1/2} \int_0^{y'} \frac{\rho}{\bar{\rho}_1} dy' \right\} (x')^{-1/2} . \quad .. \quad .. \quad .. \quad .. \quad .. \quad (8)$$

Equation (3) shows that using this co-ordinate the velocity profile u/u_1 for zero incidence is given by the first term f_0' which is the Blasius profile of incompressible flow, and that incidence introduces a term which varies sinusoidally around the cone periphery, being zero at $\Omega = 90$ deg and at $\Omega = 270$ deg.

Equation (4) shows that (to order α) the circumferential profile w/w_1 is independent of Ω, the circumferential angle (it should be noted, however, that at $\Omega = 0$ and 180 deg, both w and w_1 become zero).

2.2.2. *Displacement thickness.*—In a two-dimensional (or axisymmetric) flow, displacement thickness is usually defined in terms of mass-flow defect within the boundary layer. There is some difficulty in extending this concept to three-dimensional flow, because now there is more

than one velocity component parallel to the body surface. To overcome this difficulty it is necessary to go back to a more fundamental definition which considers the distribution of the normal velocity component (v) at the outer edge of the boundary layer. The derivation is as follows:

The initial calculation of the external inviscid flow is made neglecting the boundary layer and using the boundary condition $v = 0$ at the surface of the body. This yields a distribution of velocity $\underset{\sim}{q}_1$ at the body surface, where $\underset{\sim}{q}_1$ is the vector made up of the velocity components parallel to the surface of the body (u_1, w_1). The boundary-layer equations are now solved assuming the boundary conditions $|\underset{\sim}{q}| = 0$ at the body surface ($y = 0$) and $\underset{\sim}{q} = \underset{\sim}{q}_1$ at the outer edge of the boundary layer, $y = \delta$ (in practice, $y = \delta$ is defined as the position where $|\underset{\sim}{q}|/|\underset{\sim}{q}_1|$ is equal to some arbitrarily chosen value close to unity). The solution of the boundary-layer equations gives the distributions of all three velocity components u, v and w throughout the layer and in particular gives values of $v = v_1$ unequal to zero at $y = \delta$. These values of v_1 at $y = \delta$ are the new boundary condition to be used in any refinement of the solution for the external inviscid flow.

The displacement thickness ($\delta^\times$) of the boundary layer is now defined as the local height above the body surface of a fictitious impermeable surface which would produce, in inviscid flow, the same distribution of v_1 at $y = \delta$ as does the boundary layer itself.

Moore shows[6] that this leads to the general mathematical definition for $\delta^\times$

$$\operatorname{div}\left[\rho_1 \underset{\sim}{q}_1 \delta^\times - \int_0^\delta (\rho_1 \underset{\sim}{q}_1 - \rho \underset{\sim}{q})\, dy\right] = 0 \,. \quad .. \quad .. \quad .. \quad .. \quad (9)$$

In the case of flow over a cone at a small angle of incidence, equation (9) becomes

$$\delta^\times = \delta_x{}^\times - \alpha \frac{2A_2}{3 \sin\theta}\left(\delta_x{}^\times - \delta_\Omega{}^\times\right) \cos\Omega \,, \quad .. \quad .. \quad .. \quad (10)$$

where A_2 is defined by equation (1c) and

$$\left.\begin{aligned} \delta_x{}^\times &= \int_0^\delta \left(1 - \frac{\rho u}{\rho_1 u_1}\right) dy \\ \delta_\Omega{}^\times &= \int_0^\delta \left(1 - \frac{\rho w}{\rho_1 w_1}\right) dy \end{aligned}\right\} \,. \quad .. \quad .. \quad .. \quad .. \quad .. \quad (11)$$

Solutions of equations (10) and (11) over a range of values of $\bar{M}$ and θ are given in Refs. 1 and 5. Roughly, the change in $\delta^\times$ with incidence is in the same proportion to $\delta^\times$ at $\alpha = 0$ as is α to θ.

Now, to the first order in α, w/w_1 is independent of circumferential position (equation (4)), so that the same will apply to $\delta_\Omega{}^\times$ of equations (11). Hence equation (9) shows that the displacement thicknesses on the top and bottom generators of the cone ($\Omega = 180$ deg and $\Omega = 0$) are affected by the circumferential velocity w, even though $w = 0$ when $\Omega = 0$ or 180 deg. The significance of this fact when interpreting the subsequent experimental results is considered in Section 7.2.

2.2.3. *Skin friction.*—As in the case of displacement thickness, there are two components of skin friction: meridional and circumferential. To order α, only the former need be considered in estimating drag. Both contribute to a friction lift, but except at very low Reynolds numbers the laminar friction lift will be small compared with the pressure lift (Moore quotes an example in Ref. 5 where, for a Reynolds number of 300,000, $\theta = 10$ deg and $M = 4$, the friction lift coefficient is of order $0{\cdot}01\alpha$, whereas the pressure lift coefficient is of order α).

The local meridional skin-friction coefficient is given by[5]

$$C_{fx} = \frac{1}{\frac{1}{2}\bar{\rho}_1\bar{u}_1^2}\left(\mu\frac{\partial u}{\partial y}\right)_w$$
$$= (C_f)_{\alpha=0}\{1 - \alpha\cos\Omega \cdot K_1(\theta, M)\} \quad \ldots \quad (12)$$

(basing the coefficients on local flow conditions at $\alpha = 0$), where $K_1(\theta, M)$ can be obtained from Fig. 8 of Ref. 5.

It follows that the overall meridional skin friction up to a station x on the cone is given by

$$F_x = \bar{\rho}_1\bar{u}_1^2\int_0^x\int_0^\pi rC_{fx}\,d\Omega\,dx$$
$$= \pi\bar{\rho}_1\bar{u}_1^2\int_0^x r(C_f)_{\alpha=0}\,dx\,, \quad \ldots \quad (13)$$

where r is the cross-section radius of the cone.

This indicates that if the boundary layer is laminar up to station x for all values of Ω over the range of incidence considered, then (to order α) the overall skin friction along the cone is unchanged by incidence.

Finally, it should be noted that for a cone at incidence, meridional skin friction cannot be estimated from a momentum thickness derived from a meridional velocity profile alone (such as might be obtained from a pitot traverse), since the appropriate momentum integral equation includes terms involving the circumferential velocity profile. This applies for all values of Ω, including 0 and 180 deg.

3. *Tunnel Facilities, Models and Test Conditions.*—The tests were carried out in the supersonic tunnel of 5-in. square working-section which has continuous operation and has been described in previous boundary-layer reports (*see* Ref. 7 and earlier references contained therein). Stagnation pressures up to 5 Atm are now available at all Mach numbers greater than 3.

3.1. *Cone Models and Alignment.*—Two stainless-steel cone models were used for boundary-layer and transition measurements, one of 15 deg total angle and the other of 24·5 deg total angle. Because of the fundamental nature of these tests under zero heat-transfer conditions, it was considered that a smooth model surface completely free from joints and other imperfections associated with static-pressure holes and thermo-couples would outweigh the advantages of instrumentation. The cones were therefore machined from the solid, and an average surface finish of less than 16 microinches r.m.s. obtained.

For the purpose of verifying experimentally the static-pressure variation with cone incidence, a 15-deg hollow copper cone fitted with static-pressure points was used. This is of similar construction to the 20-deg cone described in Ref. 7.

The cones can be pitched only in the plane of expansion of the two-dimensional single-sided nozzle, the angle being adjusted by a mechanical linkage system described in Ref. 7. Cone alignment was measured optically by sighting the cone tip through grids attached to each window.

The grid interval was 0·1 in., giving an angular interval of 0·5 deg for the 15-deg cone and 0·8 for the 24·5-deg cone. The cone tip was sighted onto the lines only and not to any intermediate position, so that relative errors in alignment are not likely to have exceeded 0·1 deg.

3.2. *Test Conditions.*—Test conditions are detailed in Table 1 below. A wide range of stagnation pressure was necessary to ensure that the transition front remained on the cone at all angles of incidence (-2 deg $< \alpha < +2$ deg) and also to enable selected laminar or turbulent

boundary-layer traverses to be made from the available tunnel pitot positions. An additional test series was made to determine if tunnel stagnation pressure significantly affected transition Reynolds number.

Stagnation temperature was steady throughout each run at a value near 35 deg C.

TABLE 1

Summary of Test Conditions

Test	Cone angle (deg)	Mach number —undisturbed stream (M_∞)	Stagnation pressure (Atm)	Local Reynolds number per in. (millions)
Transition tests using azo-benzene and creeper pitot techniques	15	3·17	2·8	0·49
	15	3·82	5·1	0·68
	24·5	3·82	5·3	0·82
Static pressure measurements..	15	3·17	2·8	0·49
Pitot traverses of boundary layer	15	3·17	1 to 5	0·175 to 0·88
Effects of stagnation pressure on transition position	15	3·17	2 to 5	0·35 to 0·88

4. *Boundary-Layer Measuring Techniques.*—The extent of the laminar and turbulent boundary-layer regions was determined by the sublimation technique using a 5 per cent solution of azo-benzene in petroleum ether. The solution is sprayed on to the model and adheres as a thin crystalline coat. When exposed to an air-stream the sublimation rate is greater where the boundary layer is turbulent than where it is laminar and the two regions are thus indicated by the presence or absence of the chemical after some minutes exposure.

The azo-benzene results were checked with pitot traverses along the surfaces of the cone using a creeper pitot with a stainless-steel hypodermic tip 0·020 in. outside diameter.

Measurements normal to the boundary layer were made with quartz-tipped pitot-tubes (Ref. 8) with an outside diameter range from 0·006 to 0·010 in. Tube sizes were chosen as far as possible in accordance with the recommendations of Ref. 9 in order to reduce the effects of pitot size as much as possible.

4.1. *Effect of Cross-Flow Conditions within the Boundary Layer.*—The pitot traverses discussed in this note were all made in the plane of symmetry ($\Omega = 180$ deg) where the flow direction in the boundary layer is in the plane of symmetry. However, it is not out of place to note the implications of taking pitot readings at other points on the cone, where cross flow exists.

Consider the conditions under which the boundary layer has been measured in these tests (*i.e.*, on a 15-deg. cone at $M_\infty = 3{\cdot}17$). The theory of Ref. 5 indicates that the streamline at the outer edge of the laminar boundary layer would have a maximum inclination of approximately 1·5 deg per deg of incidence from the meridional direction and the streamline at the inner edge of the boundary layer would have a corresponding maximum inclination of about 7·5 deg per deg of incidence. These maxima occur at $\Omega = 90$ and 270 deg.

For the incidence range considered in this note (-2 deg $< \alpha < +2$ deg), it is unlikely that any significant inaccuracies would be introduced into the pitot-pressure interpretation if the pitot is aligned with a cone generator. However, for smaller cone angles and/or larger angles of incidence, special alignment of the pitot might be required with the attendent difficulties in the interpretation of the measured velocities.

5. *The Effect of Incidence on the Measured Static-Pressure Distribution.*—The distortion of the boundary layer on a cone at incidence is a result of the pressure gradients imposed by the external axially asymmetric conical flow field as described in Section 2 above.

Moore's perturbation analysis[5] of the boundary layer on a cone at small incidence uses linearised equations for the effects of incidence on the inviscid-flow field (equations (1), neglecting terms in α^2). It is therefore essential to determine how the experimental flow conditions compared with the approximate estimates.

A check of this can be obtained most easily by static-pressure measurements on the cone surface. For this purpose a 15-deg cone model not specifically designed for incidence tests was used and unfortunately the distribution of static-pressure points was such as to preclude circumferential pressure distributions from being obtained. However, a series of points was available along the top generator ($\Omega = 180$ deg) and results from these are compared with theoretical values in Fig. 3. Agreement is only fair, but the theoretical movements with incidence are substantially confirmed, the scatter of the points probably being due mainly to small imperfections in the installation of the pressure points.

At zero incidence, the variation of Mach number along the length of the cone was within $\pm \frac{1}{2}$ per cent.

6. *Transition Measurements.*—Transition measurements at incidence were carried out at different Mach numbers, Reynolds numbers and stagnation pressures (*see* Table 1). There has been some evidence from other sources that the transition Reynolds number may be affected by pressure and it was decided, therefore, to carry out some extra tests on the effect of stagnation pressure on transition Reynolds number at zero incidence. Details of these tests are given in Section 6.2.

6.1. *The Effect of Incidence on Transition.*—Typical transition pictures obtained with a 5 per cent azo-benzene solution are illustrated in Figs. 4 and 5, the effect of incidence on the transition front being clearly indicated. Good agreement is obtained between results obtained from azo-benzene pictures and from creeper pitot pressure plots (Fig. 6 shows typical results from each method). The area still covered by the azo-benzene at the end of a test is a region over which the boundary layer is completely laminar. The area 'scrubbed' clean of the indicator includes the transition region* and the region over which the boundary layer is turbulent.

Results from transition measurements at $M_\infty = 3{\cdot}17$ and $3{\cdot}82$ on the 15-deg and $24{\cdot}5$-deg cones with azo-benzene are shown in Fig. 7. The transition Reynolds number R_T is plotted for both top and bottom generators ($\Omega = 180$ and 0 deg respectively) against an incidence parameter α/θ (the value of R_T corresponds to a position at which the azo-benezene deposit terminates). The experimental data show some scatter, but since the effects of the parameters θ, p_0 and M_∞ do not show any particular trends, mean curves for both $\Omega = 0$ deg and $\Omega = 180$ deg can be drawn. The transition front is clearly very sensitive to incidence. For example, transition on the 15-deg cone at + 2-deg incidence takes place at a Reynolds number $R_T = 4{\cdot}2 \times 10^6$ on the bottom generator ($\Omega = 0$ deg) and at $R_T = 0{\cdot}87 \times 10^6$ on the top generator ($\Omega = 180$ deg).

This compares with the general value of $R_T = 2{\cdot}7 \times 10^6$ at zero incidence.

6.2. *The Effect of Stagnation Pressure on Transition.*—The first reported variation (known to the authors) of transition Reynolds number with pressure was by Potter of N.O.L.[10]. This unexplained effect occurred on spin-stabilized cone-cylinder models during tests in a firing range at $M = 3{\cdot}24$. The transition Reynolds number was halved when the ambient pressure was reduced from 1 Atm to 1/3 Atm.

* There is evidence that transition from laminar to turbulent flow takes place over a region in which patches of turbulence grow in size and coalesce as they travel downstream until the layer is completely turbulent. A time-averaging instrument (*e.g.*, a pitot-tube) at a fixed station will record some sort of mean of the variations in the transition region and will indicate a boundary layer which is apparently neither laminar nor turbulent.

Similar effects have been observed in unpublished tests on cone-cylinder and ogive-cylinder models at Mach numbers up to 2 in the 18 in. $\times$ 18 in. Tunnel at the Royal Aircraft Establishment.

In both these tests the effects of pressure gradients along the models might be significant and it is appropriate to record some results obtained with azo-benzene on the 15-deg cone at zero incidence and at $M_\infty = 3{\cdot}17$.

These are shown in Fig. 8 for a stagnation-pressure range of 2 to 5 Atm.

Hardly any effect was found, but it might be plausible to draw in a mean curve as indicated, which shows the same trend as in the tests mentioned above, but the magnitude is much less*.

7. *The Laminar Boundary Layer.*—7.1. *Measured Velocity Profiles.*—Some measured velocity profiles of the laminar boundary layer on the top generator of the cone are plotted against the non-dimensional parameter λ_L (*see* Section 2.2.1) and are compared with the theoretical profiles from equation (3) in Figs. 9a and 9b.

In general there is good agreement between all the measured and theoretical profiles. This agreement is undoubtedly better for the profiles at incidences $\alpha = +1$ deg and 0 deg, when the boundary layer is thicker, than at the negative incidences $\alpha = -1$ deg and -2 deg, but in all cases the overall thicknesses agree well with theory (at $\alpha = +2$ deg the boundary layer was turbulent at the measuring station). The increasing discrepancy as the boundary-layer thickness decreases may be a pitot-size effect. In particular, the distortion of the measured profiles near the wall is probably a low-Reynolds-number effect[9] (Reynolds number based on pitot diameter and local flow conditions within the boundary layer).

An interesting feature is the 'hump' ($u/u_1 > 1{\cdot}0$) in the theoretical profile for $\alpha = -2$ deg, which is not reproduced in the corresponding measured profile.

Now, theory[5] indicates that the effects of incidence are linear for small values of α/θ, so that the profile derivative $[\partial(u/u_1)/\partial\alpha]$ at constant λ_L should be independent of α. Experimental values of this profile derivative at $\alpha = 0$ were obtained graphically from cross-plots (such as in Fig. 10a) of the measured profiles of Fig. 9b and are compared in Fig. 10b with the theoretical estimates from equation (3). The agreement between theory and experiment is remarkably good except close to the body surface ($\lambda_L < 2$), where the experimental values are affected by the profile distortion referred to above and near the outer edge of the layer ($\lambda_L > 4$), where the values are in any case small. A check on the linearity of the effects of incidence for $\alpha \neq 0$ is given by the plots of u/u_1 against α at constant λ_L in Fig. 10a. These show that experimentally these effects may not be quite linear, but the experimental accuracy is hardly sufficient to justify a firm conclusion on this point and when all the evidence is considered, the main conclusion would be that there is very good agreement between theory and experiment over the incidence range of the tests.

Consideration of the alternative plots of the velocity profiles in Fig. 9c will be deferred to Section 7.4, following consideration of displacement thickness in Section 7.2.

7.2. *Displacement Thickness.*—The definition of displacement thickness for 3-dimensional flow has been stated in Section 2.2.2 and leads to the following expression:

$$\delta^\times = \delta_x{}^\times - \alpha \frac{2A_2}{3 \sin\theta} (\delta_x{}^\times - \delta_\Omega{}^\times) \cos\Omega \, . \qquad \ldots \qquad \ldots \qquad \ldots \qquad \ldots \qquad (10)$$

* Studies in the U.S.A. suggest that the 'stagnation-pressure effect' is in reality an effect of tip or leading-edge thickness[13,14]. Thus, unless the tip is a mathematical point, there will be a detached shock wave in its neighbourhood and local Reynolds numbers on streamlines which have come through this region will be smaller than those given by conical-flow tables. This can give an effect in the right direction when compared with the 'stagnation-pressure effect' and Bertram[13] has correlated transition results on the basis of leading-edge-thickness Reynolds number. Unfortunately the tip thickness was not measured in the present test series, but the tips were made as sharp as possible and the corresponding Reynolds numbers were probably fairly small.

Pitot traverses are suitable only for the evaluation of the meridional displacement thickness $\delta_x{}^\times$ (*see* Section 7.2.1 for results). The circumferential displacement thickness $\delta_\Omega{}^\times$ cannot be verified experimentally and the effect of this is discussed in Section 7.2.2.

7.2.1. *Measured displacement thickness* ($\delta_x{}^\times$).—A limited number of pitot traverses were taken at three positions on the top generator of the 15-deg cone ($x = 4{\cdot}8$, $6{\cdot}9$ and $8{\cdot}8$ in. and $\Omega = 180$ deg). To ensure a complete run of laminar boundary layer over the cone for an incidence range of -1 deg $< \alpha < +1$ deg, these tests were made with a stagnation pressure of 1 Atm at $M_\infty = 3{\cdot}17$.

The meridional displacement thickness $\delta_x{}^\times = \int_0^\delta \left(1 - \frac{\rho u}{\rho_1 u_1}\right) dy$ has been plotted for $\alpha = -1$, 0 and $+1$ deg in Fig. 11 with corresponding theoretical curves derived from Ref. 5. The correspondence between experimental data and theory is sufficiently good to substantiate the velocity-profile agreement and gives additional support to the theory as a whole.

7.2.2. *Estimated circumferential displacement thickness* ($\delta_\Omega{}^\times$).—Moore's theory indicates that to the first order the circumferential displacement thickness $\delta_\Omega{}^\times$ is independent of circumferential angle Ω and in accordance with equation (10) makes a contribution to the full displacement thickness $\delta^\times$ in the plane of symmetry ($\Omega = 0$ and 180 deg).

Present pitot-tube technique enables $\delta_x{}^\times$ to be measured with normal accuracy in the plane of symmetry at least, whereas $\delta_\Omega{}^\times$ cannot be measured at all. Therefore, because only one of the two contributants to displacement thickness $\delta^\times$ can be verified experimentally, it is essential to determine the order of the second term on the right-hand side of equation (10).

At $M_\infty = 3{\cdot}17$ (corresponding to the appropriate test conditions) $\delta_x{}^\times/\delta_\Omega{}^\times \doteq 1{\cdot}5$ for the top generator of a cone of 15 deg total angle. Appropriate values inserted into equation (10) give the second term a value of approximately 3 per cent of $\delta^\times$ for 1 deg of incidence, and this will be the error involved in assuming that the measured meridional displacement thickness $\delta_x{}^\times$ is equal to the full displacement thickness $\delta^\times$.

7.3. *Skin Friction.*—As mentioned in Section 2.2.3, the meridional skin friction on a cone at incidence cannot be estimated from a momentum thickness derived from a pitot traverse giving the meridional velocity profile alone. Also it would seem that the terms in the momentum equation which involve the circumferential velocities make a greater contribution to estimates of skin friction than they do to displacement thickness, so no attempt has been made to derive estimates of skin friction from the experimental results.

However, the general agreement obtained in all other respects between theory and experiment suggests that the theoretical conclusions described in Section 2.2.3 should be valid.

7.4. *An alternative Analysis of the Measured Velocity Profiles.*—In practical applications and particularly if a quick answer is required, it is not always convenient to use the reduced non-dimensional co-ordinate λ_L of Section 2.2.1. Approximate formulae are already available to estimate the boundary-layer development on a cone at zero incidence (*e.g.*, Ref. 11 in conjunction with Mangler's $\sqrt{3}$ factor) and Moore gives curves in Refs. 1 and 5 which could then be used to estimate the effects of incidence on displacement thickness and skin friction, at given Mach number and cone angle.

However, it seemed of interest to analyse the experimental velocity profiles in terms of quantities appropriate to the actual flow over the cone at $M_\infty = 3{\cdot}17$ rather than in terms of related incompressible-flow parameters, particularly since the later measurements in the turbulent boundary layer would have to be analysed in this manner. To this end the measured velocity profiles of Fig. 9a were re-plotted in Fig. 9c against the abscissa $y/\delta_x{}^\times$, where $\delta_x{}^\times$ is the experimental meridional displacement thickness of Section 7.2.1. This gives the interesting result

that the experimental profiles over the range of incidence from $\alpha = -2$ deg to $\alpha = +1$ deg are collapsed on to a single curve which is represented well by the theoretical profile for $\alpha = 0$ deg (the range of values of $\delta_x^{\times}$ involved is shown in the second illustration on Fig. 9c).

Thus, experimentally, the velocity profile

$$u/u_1 = F(y/\delta_x^{\times}) \quad .. \quad .. \quad .. \quad .. \quad .. \quad .. \quad .. \quad (14)$$

is seen to be independent of incidence over the range covered by the tests (-2 deg $\leqslant \alpha \leqslant +1$ deg), which means that although small angles of incidence alter the thickness of the laminar boundary layer by appreciable amounts, they do not alter the shape of velocity profiles measured in the plane of symmetry.

7.4.1. *Derivation of skin friction.*—If equation (14) applies, then the local meridional skin friction τ_0 is given by

$$\tau_0 = \left(\mu \frac{\partial u}{\partial y}\right)_{y=0}$$

$$= \frac{u_1 \mu_w}{\delta_x^{\times}} F'(y/\delta_x^{\times}) \quad .. \quad .. \quad .. \quad .. \quad .. \quad .. \quad (15)$$

and taking

$$C_{f_x} = \frac{1}{\frac{1}{2}\bar{\rho}_1 \bar{u}_1^2} \left(\mu \frac{\partial u}{\partial y}\right)_{y=0}$$

we can obtain (for constant Reynolds number)

$$\frac{C_{f_x}}{(C_{f_x})_{\alpha=0}} = \frac{u_1/\bar{u}_1}{\delta_x^{\times}/(\delta_x^{\times})_{\alpha=0}} . \quad .. \quad .. \quad .. \quad .. \quad .. \quad .. \quad (16)$$

Now

$$u_1/\bar{u}_1 = 1 - \alpha A_1 \cos \Omega \quad .. \quad .. \quad .. \quad .. \quad .. \quad .. \quad (1b)$$

and following Ref. 1 we may write (for constant Reynolds number)

$$\delta_x^{\times}/(\delta_x^{\times})_{\alpha=0} = 1 - \alpha A_1 \cos \Omega \quad K_2(\theta, M) , \quad .. \quad .. \quad .. \quad .. \quad (17)$$

where $K_2(\theta, M)$ is a function of θ and M, so that substituting from equations (1*b*) and (17) in equation (16), we obtain

$$\frac{C_{f_x}}{(C_{f_x})_{\alpha=0}} = 1 + \alpha \cos \Omega \, . \, A_1\{K_2(\theta, M) - 1\} . \quad .. \quad .. \quad .. \quad (18)$$

Under the conditions of the present tests both theory and experiment support

$$\frac{\delta_x^{\times}}{(\delta_x^{\times})_{\alpha=0}} = 1 - 10{\cdot}55\alpha \cos \Omega .. \quad .. \quad .. \quad .. \quad .. \quad .. \quad (17a)$$

and, from the inviscid-flow tables[2], $A_1 = 0{\cdot}204$, so that equation (18) gives

$$\frac{C_{f_x}}{(C_{f_x})_{\alpha=0}} = 1 + 10{\cdot}35\alpha \cos \Omega , \quad .. \quad .. \quad .. \quad .. \quad .. \quad (18a)$$

which compares with the theoretical relation

$$\frac{C_{f_x}}{(C_{f_x})_{\alpha=0}} = 1 + 11{\cdot}17\alpha \cos \Omega \quad .. \quad .. \quad .. \quad .. \quad .. \quad (18b)$$

from Ref. 5. Since α is in radians, the percentage difference between these formulae will be small when α is small. Furthermore, comparison with the curves for $\delta_x^{\times}$ and C_{f_x} in Ref. 5 shows that equation (18) gives equally good results over the whole range of Mach numbers (up to 5)

and cone angles (total angles between 20 and 60 deg) considered by Moore (it happens that the agreement is improved if the term $u_1/\bar{u}_1$ is taken as unity in equation (16), which simplifies the procedure).

Physically this means that the local skin friction at any point increases with incidence roughly at the same rate as the displacement thickness decreases and *vice versa*.

8. *The Turbulent Boundary Layer.*—There is no theory for the turbulent boundary layer to correspond with Moore's theory for the laminar boundary layer on bodies at incidence, so pitot traverses in the turbulent layer on the 15-deg cone at $M_\infty = 3{\cdot}17$ have been analysed along the lines of the alternative analysis of the laminar boundary-layer measurements in Section 7.4.

8.1. *Velocity Profiles.*—Fig. 12 shows turbulent velocity profiles derived from pitot traverses at three stations along the top generator of the cone for cone incidences ranging from — 2 to + 2 deg. These are plotted against $y/\delta_x{}^\times$, where $\delta_x{}^\times$ is the experimentally determined meridional component of displacement thickness, and when the flow is fully turbulent this gives a good correlation of all the experimental profiles. Throughout most of the boundary layer these are also in good agreement with the turbulent power-law profile

$$u/u_1 = (y/\delta)^{1/7} \quad .. \quad .. \quad .. \quad .. \quad .. \quad .. \quad .. \quad (19)$$

with the value of $(\delta^\times/\delta)$ appropriate to the test conditions and a 1/7-power-law profile (read from the curves of Ref. 12).

Thus (as was the case with a laminar boundary layer), it would seem that small angles of incidence may alter the thickness of the turbulent boundary layer, but do not affect the shape of the velocity profile. The alternations in thickness are considered in the following Sub-section.

8.2. *Displacement Thickness.*—Corresponding to a 1/7-power-law velocity profile, experimental evidence (e.g., Ref. 7) supports the variation of displacement thickness* with distance along the body given by

$$\delta^\times = k(x - x_0)/(R_{x-x_0})^{1/5}, \quad .. \quad .. \quad .. \quad .. \quad .. \quad (20)$$

where x_0 is the distance from the leading edge to the 'effective start' of the turbulent boundary layer.

Unfortunately the cone was not long enough to enable reliable sets of measurements of $\delta^\times$ to be obtained at one stagnation pressure alone and when stagnation pressure is altered, both the Reynolds number per inch and the value of x_0 are changed. To compensate for this, equation (20) was used in the alternative form.

$$R_{\delta^\times} = k(R_{x-x_0})^{4/5}, \quad .. \quad .. \quad .. \quad .. \quad .. \quad .. \quad (21)$$

where

$$R_{\delta^\times} = \frac{\bar{\rho}_1 \bar{u}_1 \delta^\times}{\bar{\mu}_1}$$

$$R_{x-x_0} = \frac{\bar{\rho}_1 \bar{u}_1 (x - x_0)}{\bar{\mu}_1};$$

thus

$$R_{\delta^\times} = k(R_x - R_{x0})^{4/5}. \quad .. \quad .. \quad .. \quad .. \quad .. \quad .. \quad (21a)$$

It was then assumed that, at a given incidence, R_{x_0} would not alter with stagnation pressure, which assumption would be justified if transition Reynolds number remained constant. The azo-benzene test results of Fig. 8 show that there may in fact have been a small increase in

* From this point onwards, 'displacement thickness' will be taken to mean the 'meridional displacement thickness' and will be denoted $\delta^\times$. This is to avoid confusion in the mathematical manipulations.

transition Reynolds number as stagnation pressure increased, so some error may be expected from this cause. For reasons of this nature the following results for the turbulent boundary layer are probably less accurate than their laminar counterparts discussed previously.

Taking R_{x_0} to be constant in equation (21*a*) results in a single curve of $R_{\delta\times}$ against R_{x-x_0} for all stagnation pressures. However, R_{x_0} is an unknown to be determined from the test results and this is done most easily by plotting $(R_{\delta\times})^{5/4}$ against R_x as in Fig. 13, i.e., equation (21*a*) is used in the form

$$(R_{\delta\times})^{5/4} = k^{5/4}(R_x - R_{x_0}) \quad .. \quad .. \quad .. \quad .. \quad .. \quad .. \quad (21b)$$

and by this plot the experimental results for a given incidence should lie on a straight line.

The experimental results in Fig. 13 are taken mainly from traverses at the last two stations on the cone ($x = 6{\cdot}9$ and $8{\cdot}8$ in.) at stagnation pressures between $2\frac{1}{2}$ and 5 Atm. A number of results showed unexplained inconsistencies, lying well away from the mean lines of Fig. 13, but in these cases the velocity profiles did not agree with the 1/7-power profile of Fig. 12, so they have not been included (these inconsistent results were not confined to any particular incidence and among the causes may have been disturbances arising from removable plugs in the liner upstream of the station where the pitot traverses were being made. These plugs seal the holes through which pitot-tubes can be inserted into the tunnel (*see* Ref. 7)).

The experimental results in Fig. 13 therefore correspond to consistent velocity profiles and are given for two values of incidence, $\alpha = 0$ deg and $\alpha = +2$ deg. They can be fitted well by straight lines in accordance with equation (21*b*) and when transformed back to equation (21) the equations for displacement thickness are

$$R_{\delta\times} = 0{\cdot}072(R_{x-x_0})^{4/5}, \quad .. \quad .. \quad .. \quad .. \quad .. \quad .. \quad (22)$$

when $\alpha = 0$ deg, with $R_{x_0} = 1{\cdot}25 \times 10^6$

and

$$R_{\delta\times} = 0{\cdot}084(R_{x-x_0})^{4/5} \quad .. \quad .. \quad .. \quad .. \quad .. \quad .. \quad (23)$$

when $\alpha = +2$ deg, with $R_{x_0} = 0{\cdot}2 \times 10^6$.

From equations (22) and (23), and assuming a linear variation of $R_{\delta\times}$ with α at constant R_{x-x_0}, we obtain

$$R_{\delta\times}/(R_{\delta\times})_{\alpha=0} = 1 + 4{\cdot}8\alpha \quad .. \quad .. \quad .. \quad .. \quad .. \quad .. \quad .. \quad (24)$$

(with α in radians) for the turbulent boundary layer on the upper generator of a 15-deg cone at $M_\infty = 3{\cdot}17$, which compares with

$$R_{\delta\times}/(R_{\delta\times})_{\alpha=0}\ 1 + 10{\cdot}55\alpha \quad .. \quad .. \quad .. \quad .. \quad .. \quad .. \quad (17b)$$

from equation (17*a*) for a laminar boundary layer under the same conditions.

Thus it seems that, in percentages, small angles of incidence have less than half the effect on the growth of turbulent boundary layers than they have on laminar boundary layers. The experimental accuracy would hardly justify searching for more detailed conclusions either as regards the development of the turbulent boundary layer on a cone at $\alpha = 0$ or as regards the effects of incidence.

9. *Conclusions.*—A test series investigating the boundary layer on cones at incidence in a supersonic airstream under zero heat-transfer conditions led to the following conclusions:

(1) Static-pressure measurements along the upper generator of a 15-deg cone at $M_\infty = 3{\cdot}17$ were in reasonable agreement with theoretical values given by the M.I.T. Tables (Ref. 2) within the incidence range of the tests (-2 deg $\leqslant \alpha \leqslant +2$ deg) (*see* Fig. 3).

(2) Cross flow within the boundary layer renders its growth and stability axially asymmetric. A result of this is considerable distortion of the transition front, which was measured with an azo-benzene technique on the 15-deg and 24·5-deg (total angle) cones at $M_\infty = 3{\cdot}17$ and 3·89 (Fig. 5). Mach number had little effect and the effect of cone angle could be eliminated by plotting the results against α/θ, where α is incidence and θ is the semi-angle of the cone (Fig. 7). A typical result was that at 2-deg incidence there was a ratio of 4 to 1 between the transition Reynolds numbers on the bottom and top generators of the 15-deg cone.

(3) A check of the effect of stagnation pressure on transition Reynolds number on the 15-deg cone at $M_\infty = 3{\cdot}17$ showed only a slight increase in transition Reynolds number as the stagnation pressure was increased from 2 to 5 Atm (Fig. 8).

(4) Pitot traverses of the laminar boundary layer along the top generator of the 15-deg cone were analysed on the basis of Moore's theory[1,5]. Remarkably good agreement was obtained between experimental and theoretical velocity profiles (Fig. 9a) and in their derivatives with respect to incidence (Fig. 10). Fig. 9c shows that small angles of incidence alter the thickness of the boundary layer, but do not have any marked effect on the shape of velocity profiles measured in the plane of symmetry.

(5) Displacement thicknesses derived from the pitot traverses were in good agreement with the theoretical estimates[5] (Figs. 9c and 11).

(6) Measurements of the turbulent boundary layer showed that the shape of the velocity profile in the plane of symmetry was not affected by incidence (Fig. 12).

(7) The derived variations of displacement thickness of the measured turbulent boundary layers (Fig. 13) are considered to be less accurate than those obtained for the laminar boundary layer, but, on the evidence of Fig. 13, small angles of incidence had less than half the effect on the growth of the turbulent boundary layer than they had on the growth of a laminar boundary layer (Figs. 9c and 11).

LIST OF SYMBOLS

$A_1, A_2 A_3$ — Functions of θ and M specifying first-order effects of incidence on the external inviscid flow (*see* Section 2.1, equations (1))

B_1, B_3, D_1, D_2, D_3 — Functions of θ and M specifying second-order effects of incidence on the external inviscid flow (*see* Section 2.1, equations (1))

C — Constant in the viscosity-temperature relation $\mu/\mu_r = C\dfrac{T}{T_r}$

F — Function defining the laminar velocity profile $u/u_1 = F(y/\delta^*)$ (*see* Section 7.4, equation (14))

K_1, K_2 — Functions of θ and M, appearing in equations (12) and (17)

M — Mach number

R — Reynolds number based on $\bar{u}_1$, $\bar{\rho}_1$ and $\bar{\mu}_1$

T — Temperature

T_w — Temperature at body surface (wall)

$X = \dfrac{\bar{\rho}_1\bar{u}_1}{\bar{\mu}_1 C}x$

$Y = \sqrt{3}(p/\bar{p})^{-1/2}\displaystyle\int_0^{y'}\frac{\rho}{\bar{\rho}_1}dy'$ with $y' = \dfrac{\bar{\rho}_1\bar{u}_1}{\bar{\mu}_1 C}y$

C_{f_x} — Local meridional skin-friction coefficient $= \tau_0/\frac{1}{2}\bar{\rho}_1\bar{u}_1^2$

f — Component of vector potential related to the meridional velocity u in the boundary layer

f_0 — Value of f for $\alpha = 0$

h_1, h_2, h_3 — Functions involving first-order perturbation potentials related to the meridional and circumferential velocities u and w in the boundary layer

p — Static pressure

p_0 — Stagnation pressure

$\underset{\sim}{q}$ — The velocity vector (u, w)

$|\underset{\sim}{q}|$ — Modulus of $\underset{\sim}{q} = \sqrt{(u^2 + w^2)}$

r — Radius of cone cross-section

u — Velocity component in direction of x

v — Velocity component in direction of y

w — Circumferential component of velocity

x — Co-ordinate along cone generators (meridional)

x_0 — Value of x at effective start of the turbulent boundary layer

y — Co-ordinate normal to cone surface

α — Angle of incidence

γ	Ratio of specific heats
δ	Boundary layer ' thickness '
$\delta^\times$	Displacement thickness defined by equation (9), Section 2.2.2
$\delta_x{}^\times$	Displacement thickness associated with the u-profile
$=$	$\int_0^\delta \left(1 - \frac{\rho u}{\rho_1 u_1}\right) dy$
$\delta_\Omega{}^\times$	Displacement thickness associated with the w profile
$=$	$\int_0^\delta \left(1 - \frac{\rho w}{\rho_1 w_1}\right) dy$
θ	Semi-angle of cone
μ	Viscosity
ρ	Density
τ_0	Local meridional skin friction $= \left(\mu \frac{\partial u}{\partial y}\right)_{y=0}$
Ω	Circumferential angular co-ordinate measured from bottom generator of cone

Suffices

$_r$	Reference condition
$_x$	Related to direction or distance
$_T$	Related to value of x at transition
$_{\delta^\times}$	Related to displacement thickness $\delta_x{}^\times$
$_1$	Local conditions just outside the boundary layer
$_\infty$	Undisturbed stream ahead of the body

Superscript

$\bar{}$	Denotes conditions at zero incidence

REFERENCES

No.	Author	Title, etc.
1	F. K. Moore	Three-dimensional laminar boundary-layer flow. *J. Ae. Sci.* Vol. 20. No. 8. pp. 525 to 534. August, 1953.
2	—	Tables of supersonic flow around yawing cones. Massachusetts Institute of Technology. Elec. Eng. Dept. Tech. Reports 3 and 5. 1947 and 1949.
3	G. B. W. Young and C. P. Siska	Supersonic flow around cones at large yaw. *J. Ae. Sci.* Vol. 19. No. 2. pp. 111 to 119. February, 1952.
4	F. K. Moore	Three-dimensional compressible laminar boundary-layer flow. N.A.C.A. Tech. Note 2279. March, 1951.
5	F. K. Moore	Laminar boundary layer on a circular cone in supersonic flow at a small angle of attack. N.A.C.A. Tech. Note 2521. October, 1951.
6	F. K. Moore	Displacement effect of a three-dimensional boundary layer. N.A.C.A. Report 1124. (Supersedes N.A.C.A. Tech. Note 2722.) 1953.
7	F. V. Davies and J. R. Cooke..	Boundary layer measurements on 10-deg and 20-deg cones at $M = 2{\cdot}45$ and zero heat transfer. C.P. 264. November, 1954.
8	J. R. Cooke	The use of quartz in the manufacture of small diameter pitot-tubes. C.P. 193. December, 1954.
9	R. J. Monaghan	The use of pitot-tubes in the measurement of laminar boundary layers in supersonic flow. R. & M. 3056. September, 1955.
10	J. L. Potter	New experimental investigations of friction drag and boundary-layer transition on bodies of revolution at supersonic speeds. Paper presented at the 2nd Bureau of Ordnance Symposium on Aeroballistics, Pasadena, Calif. May, 1952.
11	R. J. Monaghan	An approximate solution of the compressible laminar boundary layer on a flat plate. R. & M. 2760. November, 1949.
12	W. F. Cope	Notes and graphs for boundary calculations in compressible flow. C.P. 89. August, 1951.
13	M. H. Bertram	Exploratory investigation of boundary-layer transition on a hollow cylinder at a Mach number of 6·9. N.A.C.A. Tech. Note 3546. May, 1956.
14	W. E. Moeckel	Some effects of bluntness on boundary-layer transition and heat transfer at supersonic speeds. N.A.C.A. Tech. Note 3653. March, 1956.

(76074) B

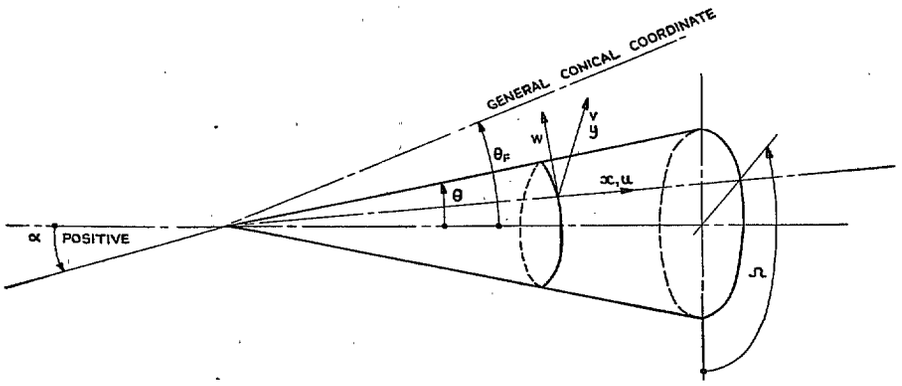

FIG. 1. Diagram of co-ordinates and symbols.

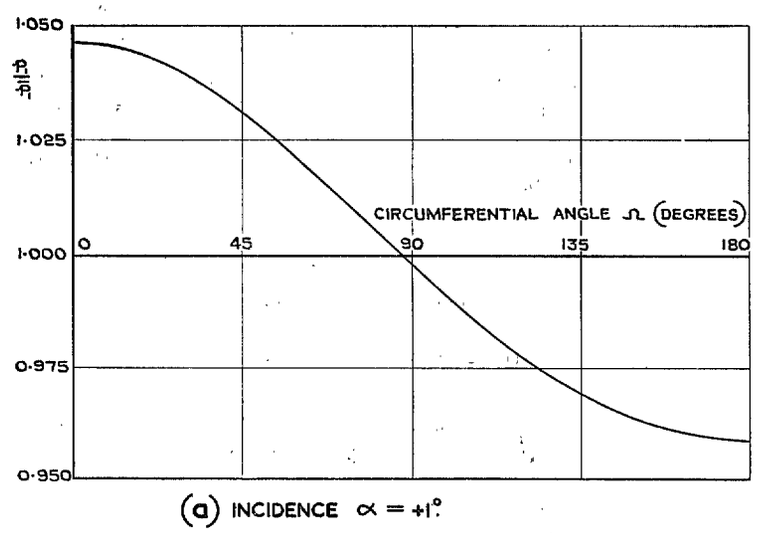

FIGS. 2a and 2b. Theoretical pressure distributions around a 15-deg (total angle) cone at incidence for $M_\infty = 3 \cdot 18$.

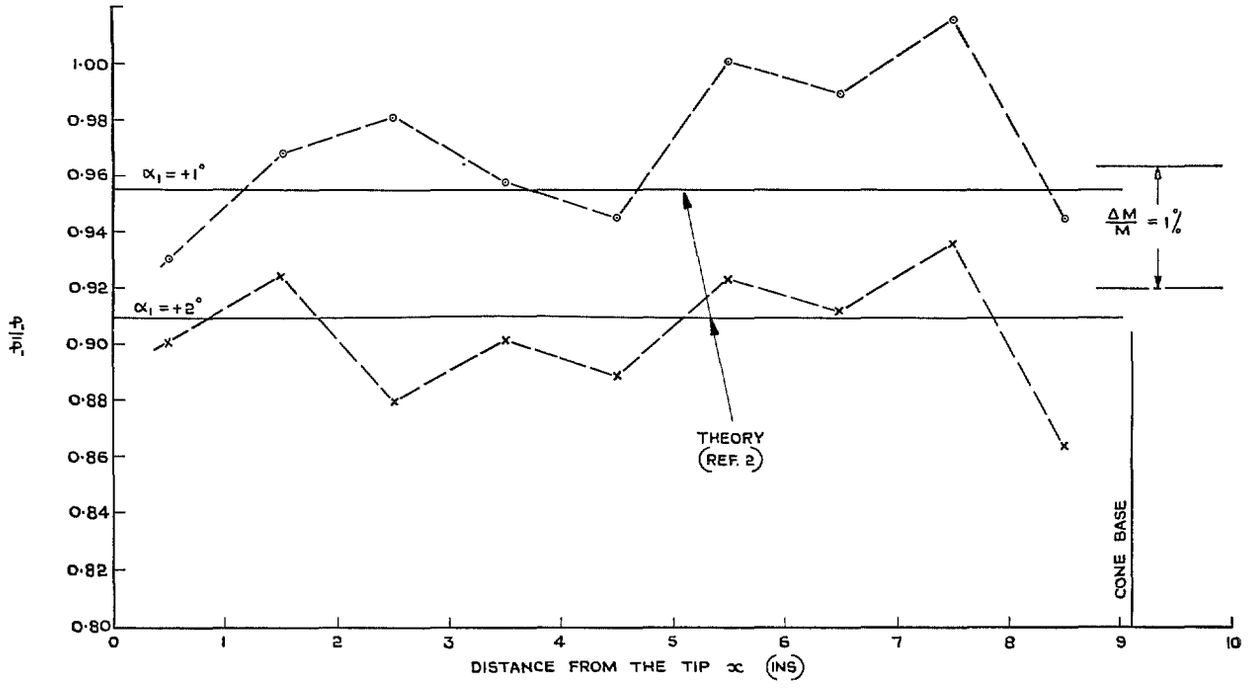

FIG. 3. Static-pressure distribution along the top generator of a 15-deg cone at incidence ($M_\infty = 3 \cdot 17$).

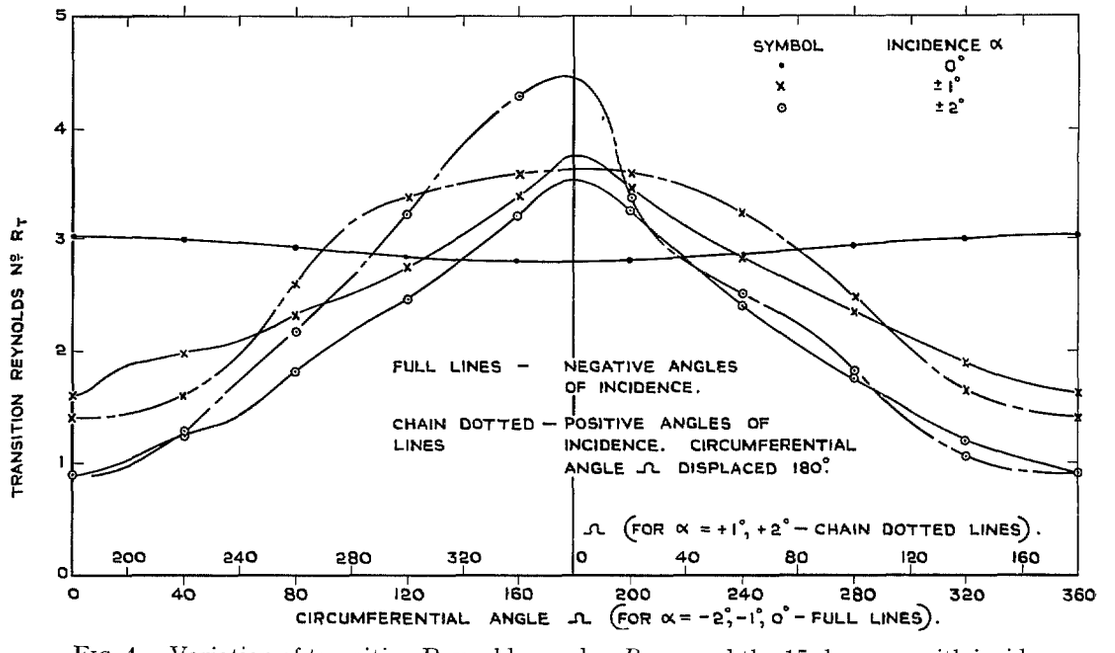

FIG. 4. Variation of transition Reynolds number R_T around the 15-deg cone with incidence.

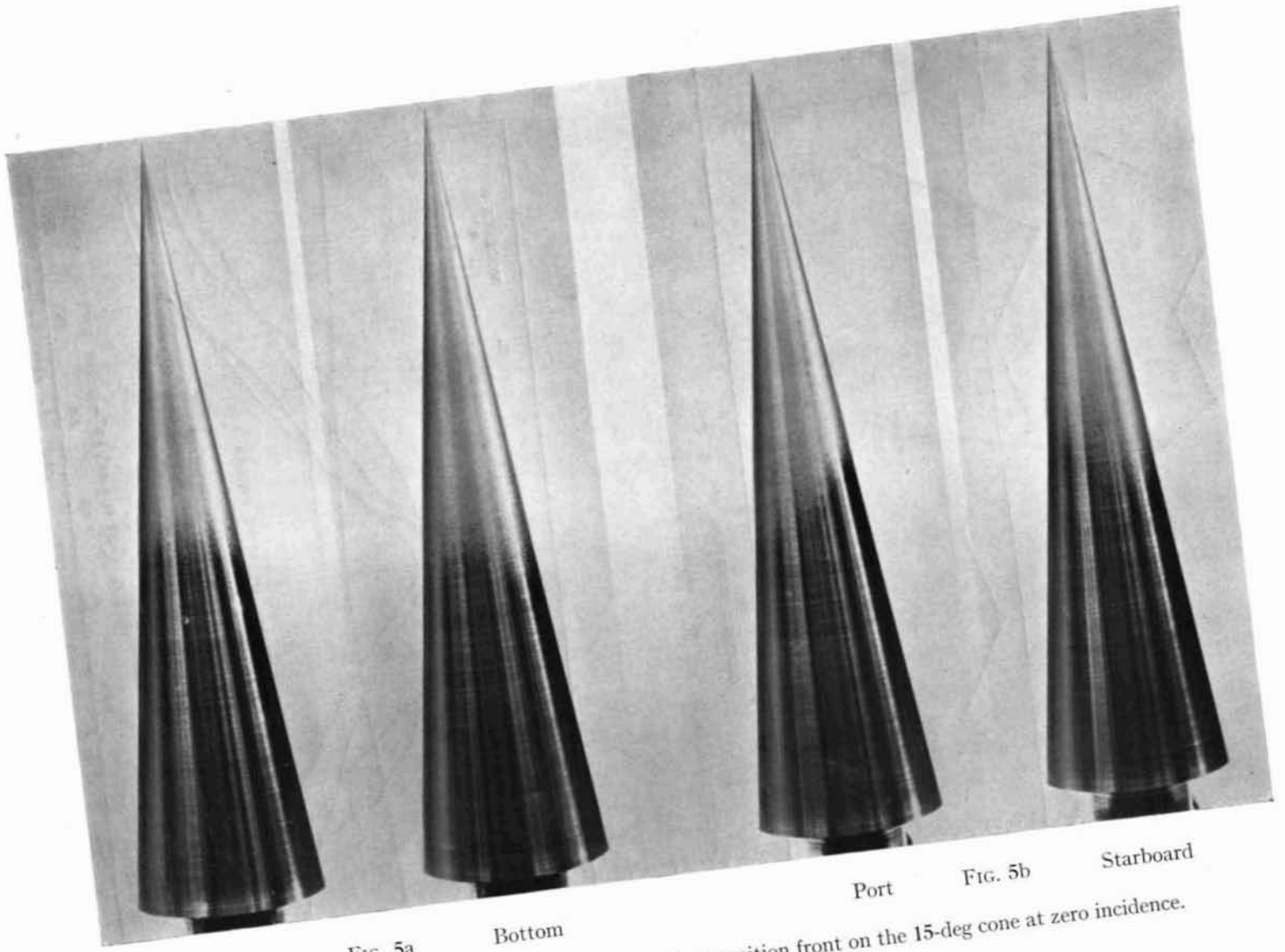

Top Fig. 5a Bottom Port Fig. 5b Starboard

Figs. 5a and 5b. Azo-benzene pictures showing the transition front on the 15-deg cone at zero incidence.

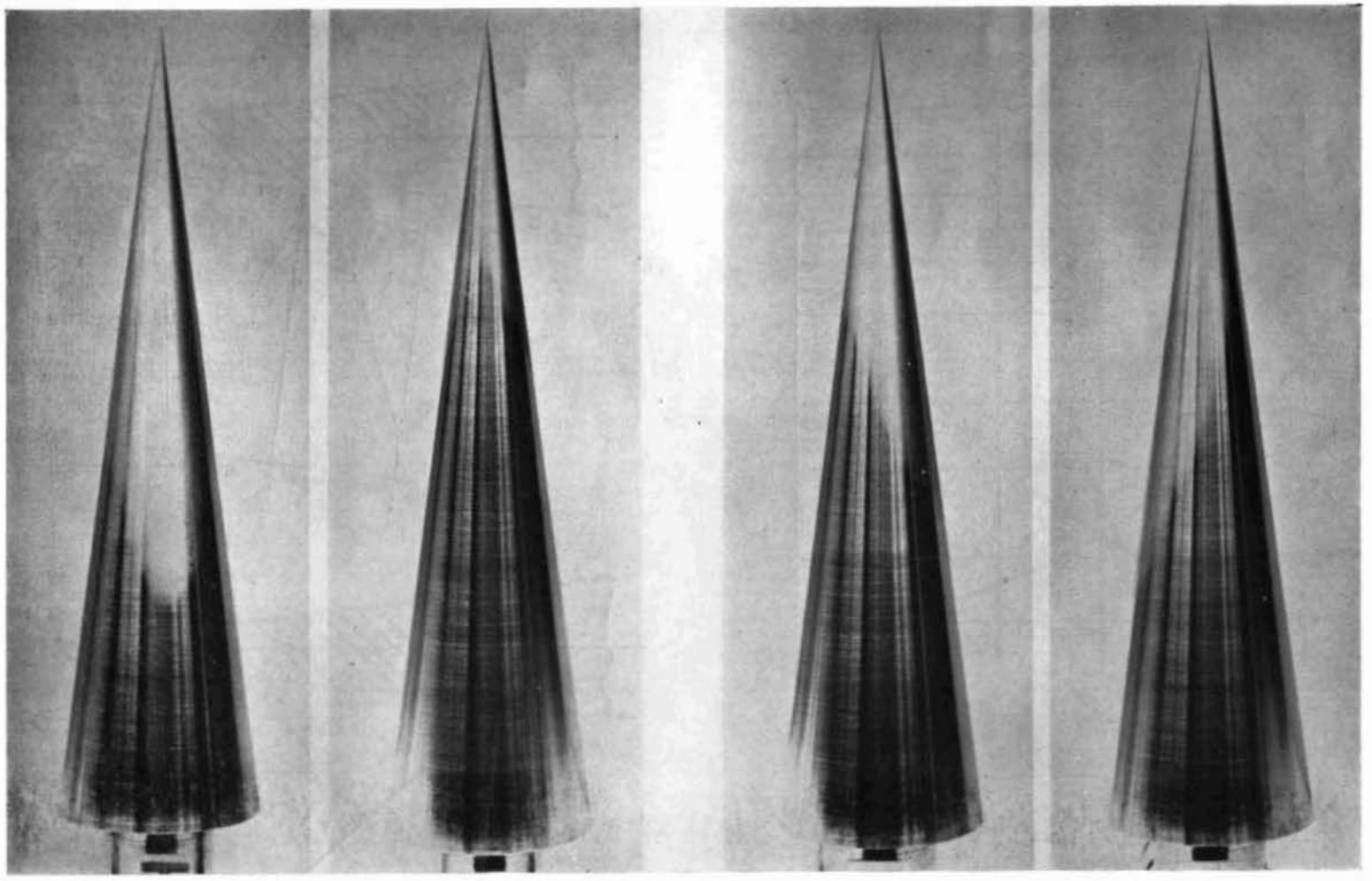

Top FIG. 5c. Bottom Port FIG. 5d. Starboard

FIGS. 5c and 5d. Azo-benzene pictures showing the transition front on the 15-deg cone at — 1-deg incidence.

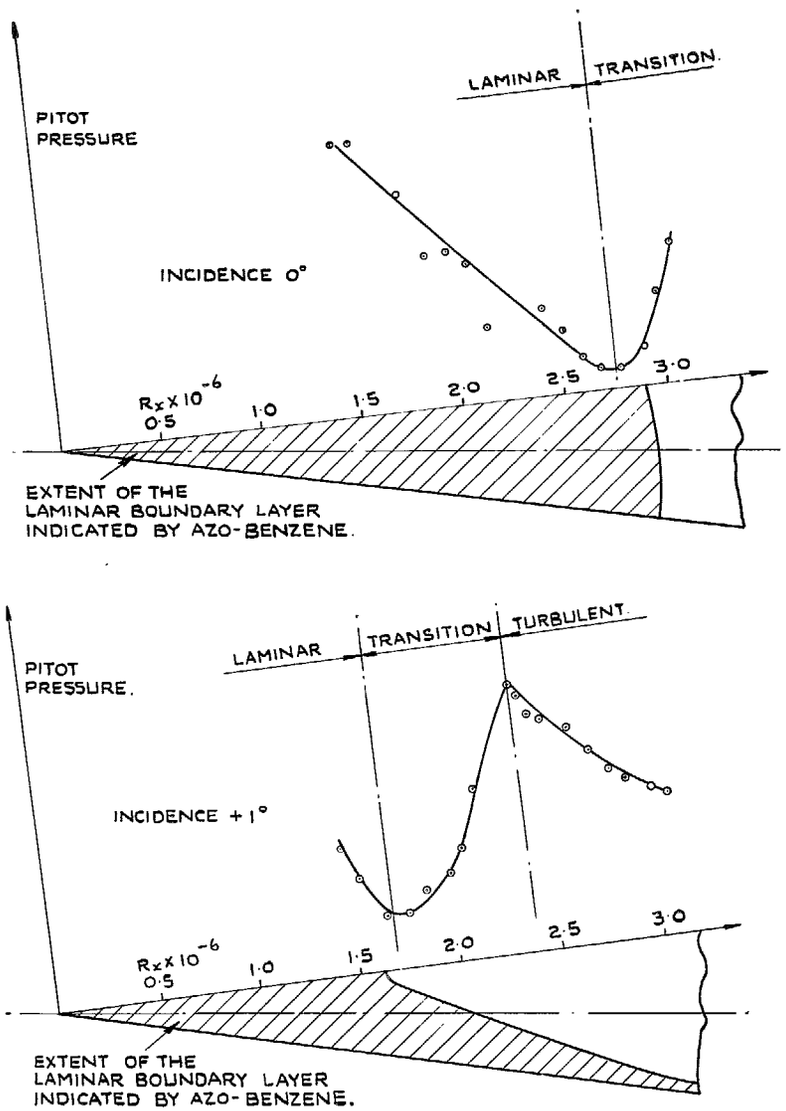

FIG. 6. Comparison between the indication of transition by azo-benzene and pressure distributions obtained from a creeper pitot traverse along the top generator of a 15-deg cone ($M_\infty = 3{\cdot}17$).

SYMBOL		CONE ANGLE	MACH Nº	STAGNATION PRESSURE
TOP GENERATOR	BOTTOM GENERATOR	2θ	M_∞	P_0 (ATMOS)
×	○	15°	3·17	2·8
⊛	⊙	15°	3·82	5·1
⊛	⊙	24·5°	3·82	5·3

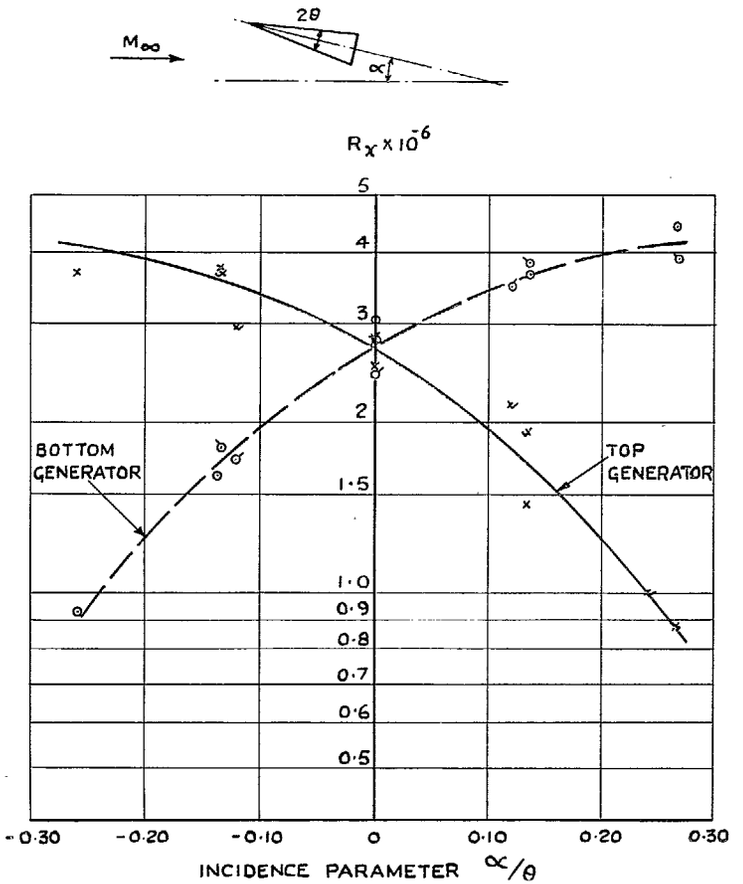

FIG. 7. Effect of incidence on boundary-layer transition on top and bottom generators of cones at incidence (Azo-benzene detection).

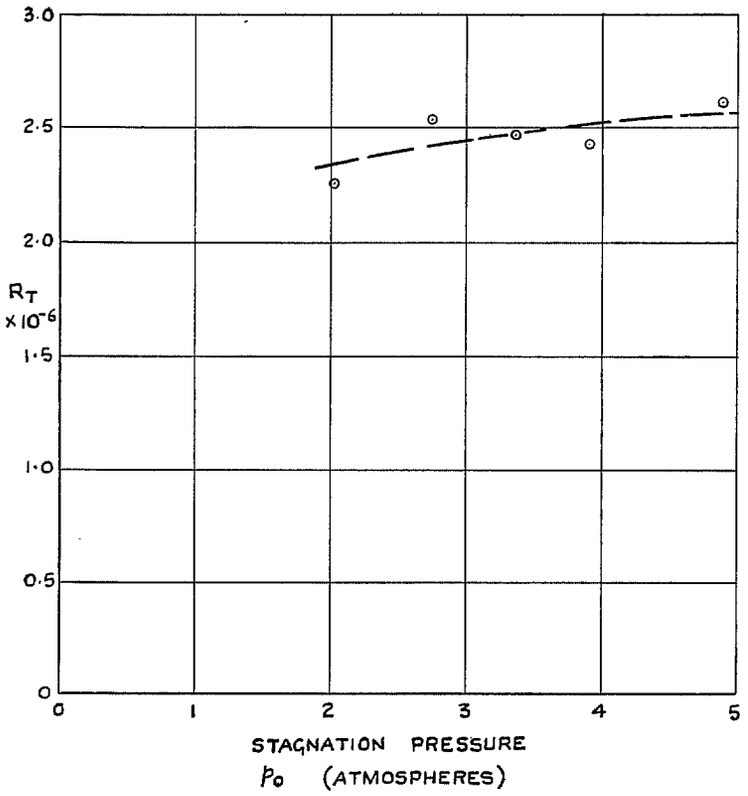

FIG. 8. Variation of transition Reynolds number R_T with tunnel stagnation pressure ($M_\infty = 3{\cdot}17$; $\alpha = 0$).

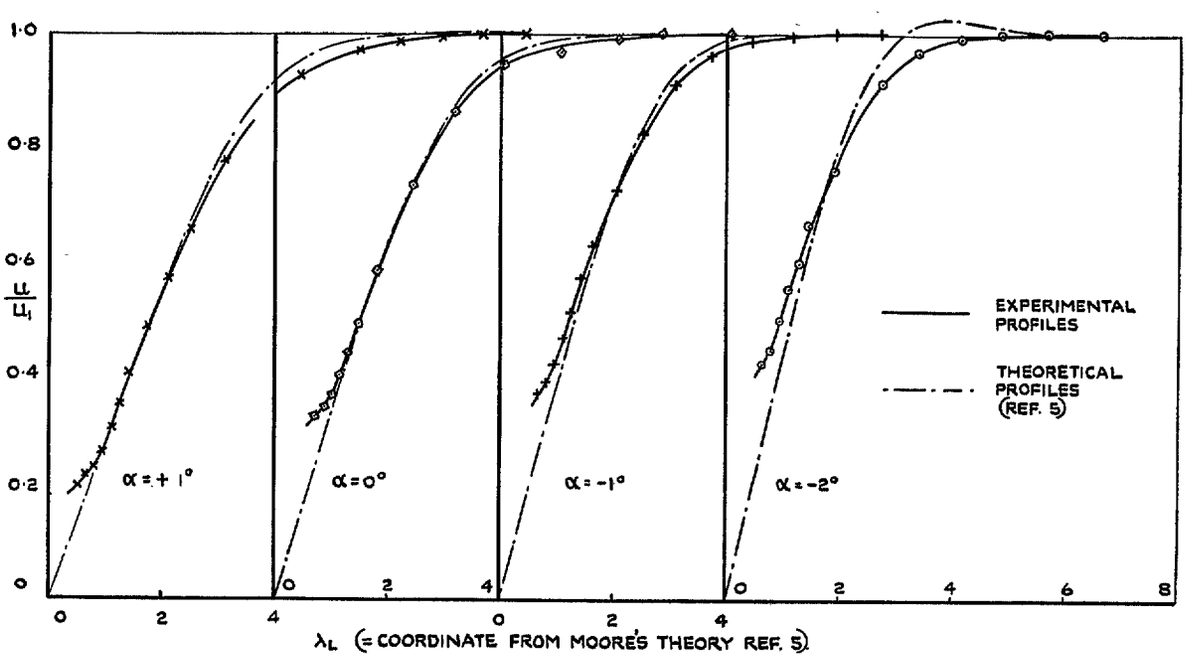

FIG. 9a. Velocity profiles of laminar boundary layers on the top generator ($\Omega = 180$ deg) of a 15-deg cone at incidence ($M_\infty = 3{\cdot}17$; $x = 4{\cdot}8$ in. $R_x = 0{\cdot}84 \times 10^6$ at $\alpha = 0$ deg).

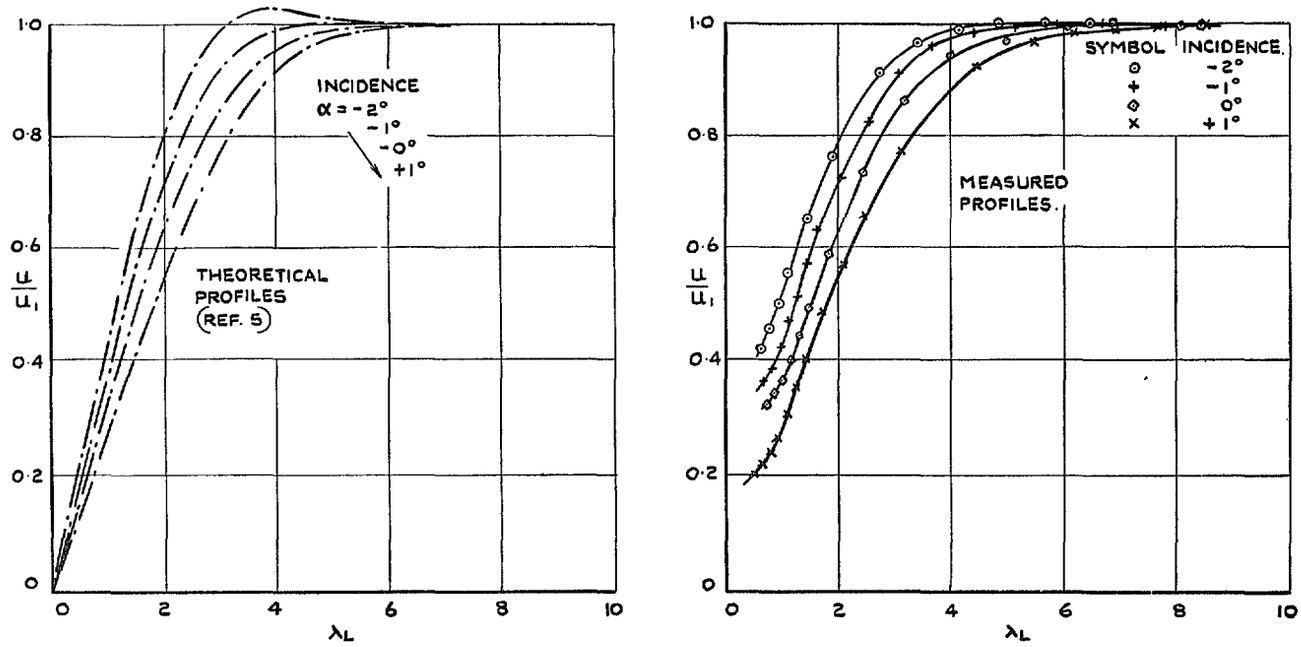

FIG. 9b. Velocity profiles of FIG. 9a showing the effect of incidence.

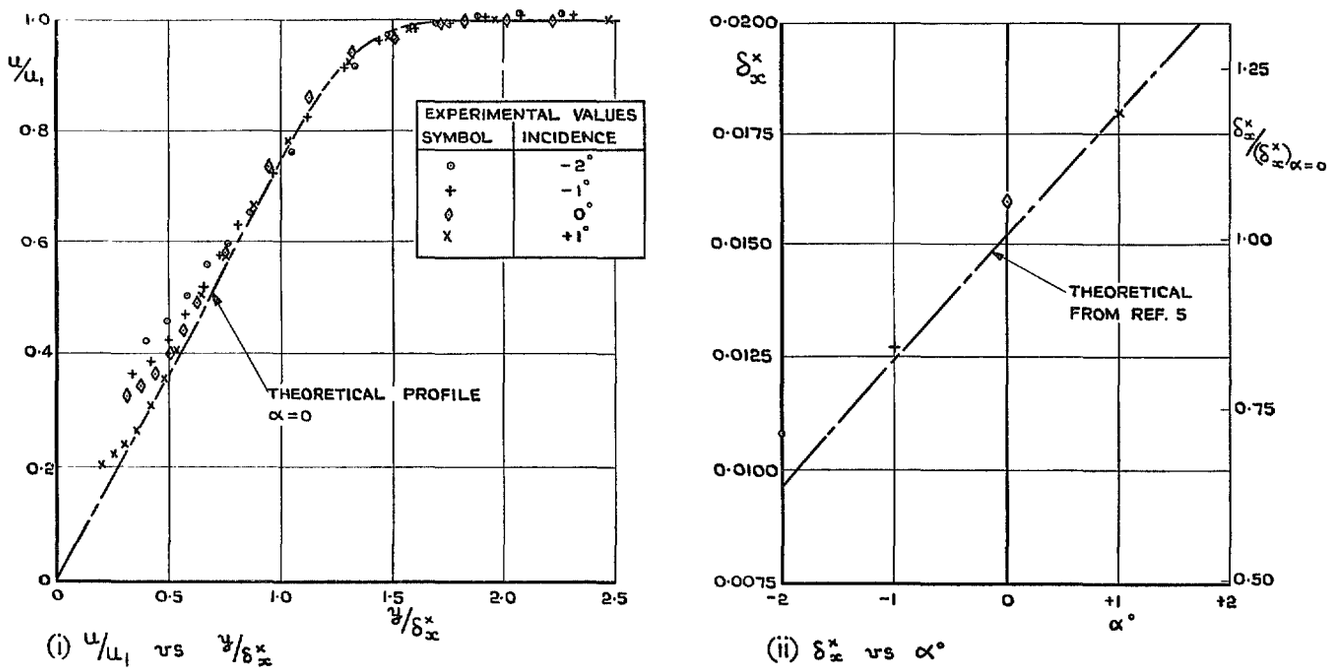

FIG. 9c. (i) Velocity profiles of FIG. 9a plotted against y/δ^x and (ii) variation of δ^x with α.

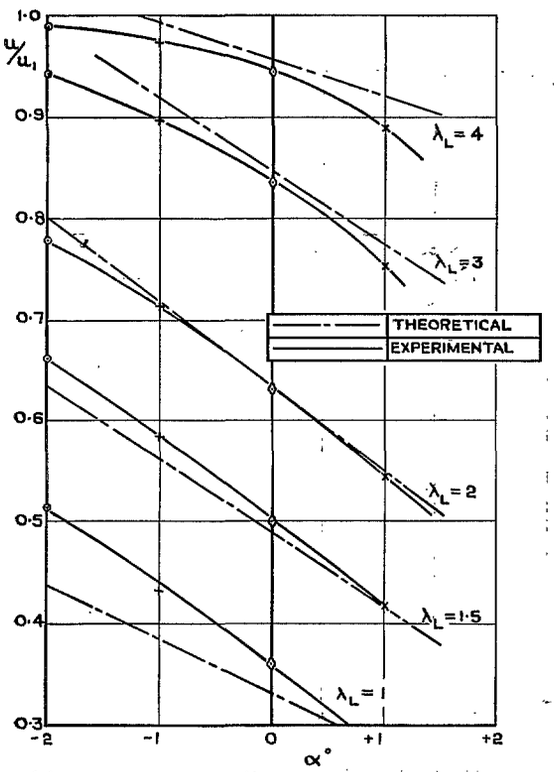

(a) VARIATION OF u/u_1 WITH α AT CONSTANT λ_L.

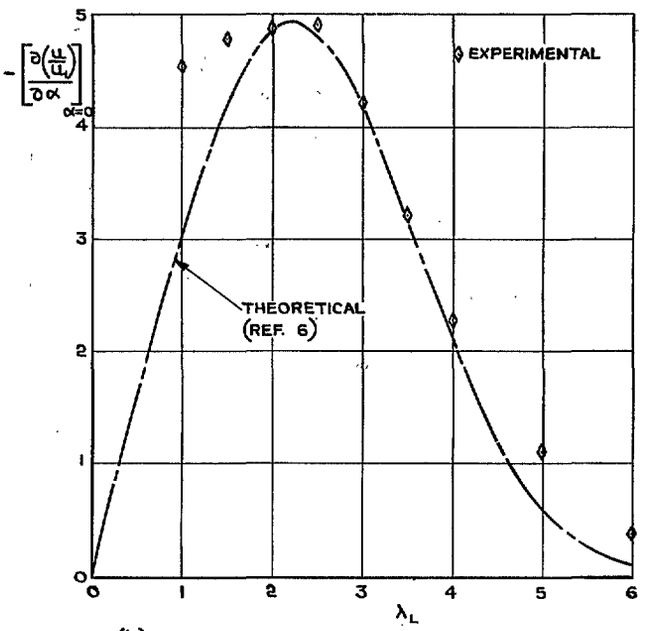

(b) PROFILE DERIVATIVES AT $\alpha = 0$.

FIGS. 10a and 10b. Check of linearity of incidence effect on velocity profile of laminar boundary layer on top generator ($\Omega = 180$ deg) of 15-deg cone ($M_\infty = 3{\cdot}17$; $R_x = 0{\cdot}81 \times 10^6$ at $\alpha = 0$ deg).

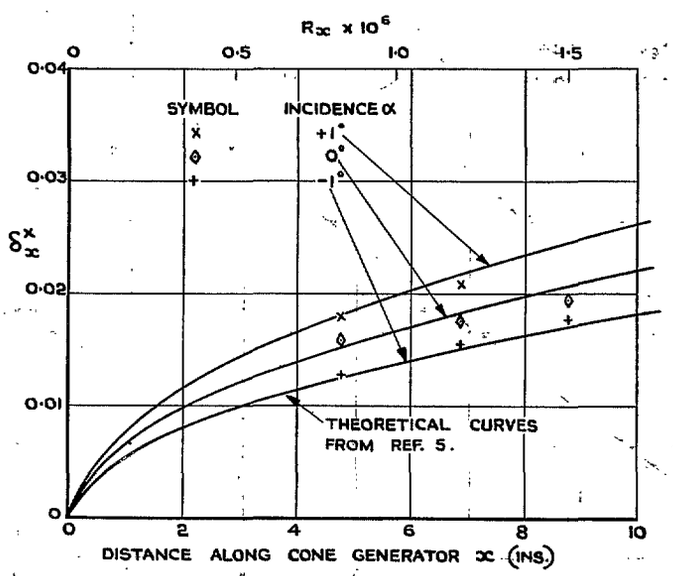

FIG. 11. Variation of meridional displacement thickness $\delta_x{}^{\times} = \int_0^{\delta} \left(1 - \frac{\rho u}{\rho_1 u_1}\right) dy$ along the top generator of the 15-deg cone ($M_\infty = 3{\cdot}17$; $R = 0{\cdot}175 \times 10^6$ per inch).

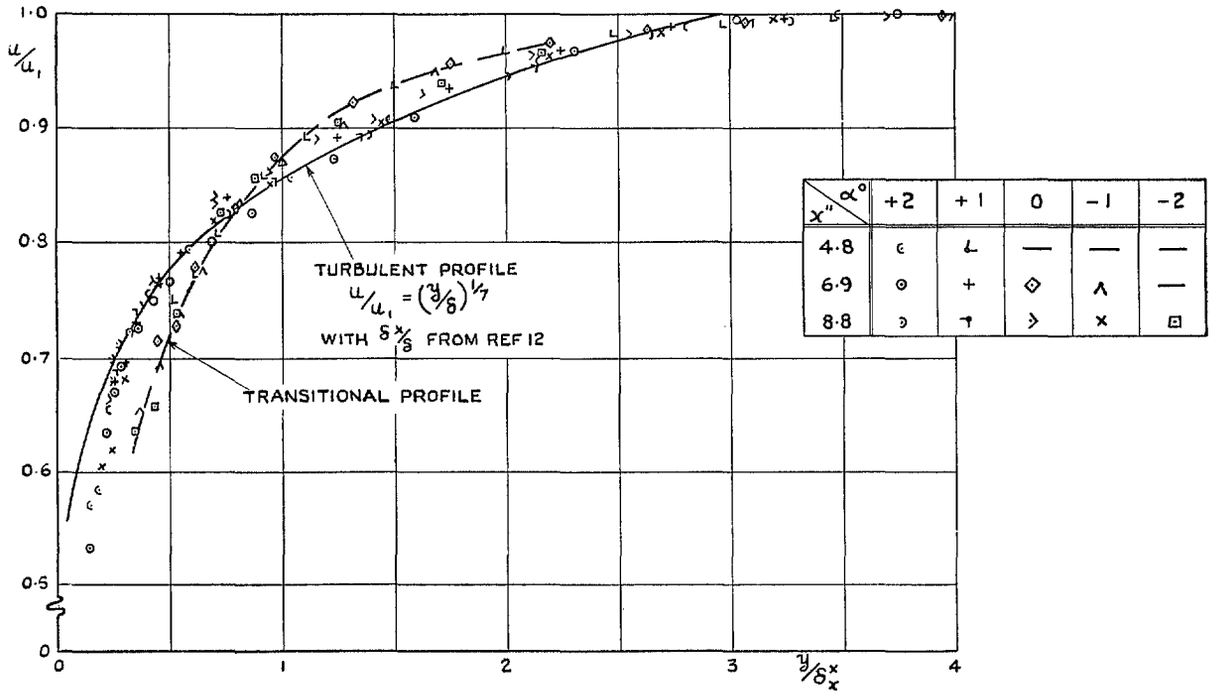

FIG. 12. Experimental velocity profiles for the turbulent boundary layer on the top generator ($\Omega = 180$ deg) of a 15-deg cone ($M_\infty = 3 \cdot 17$; $R \simeq 0 \cdot 5 \times 10^6$ per inch).

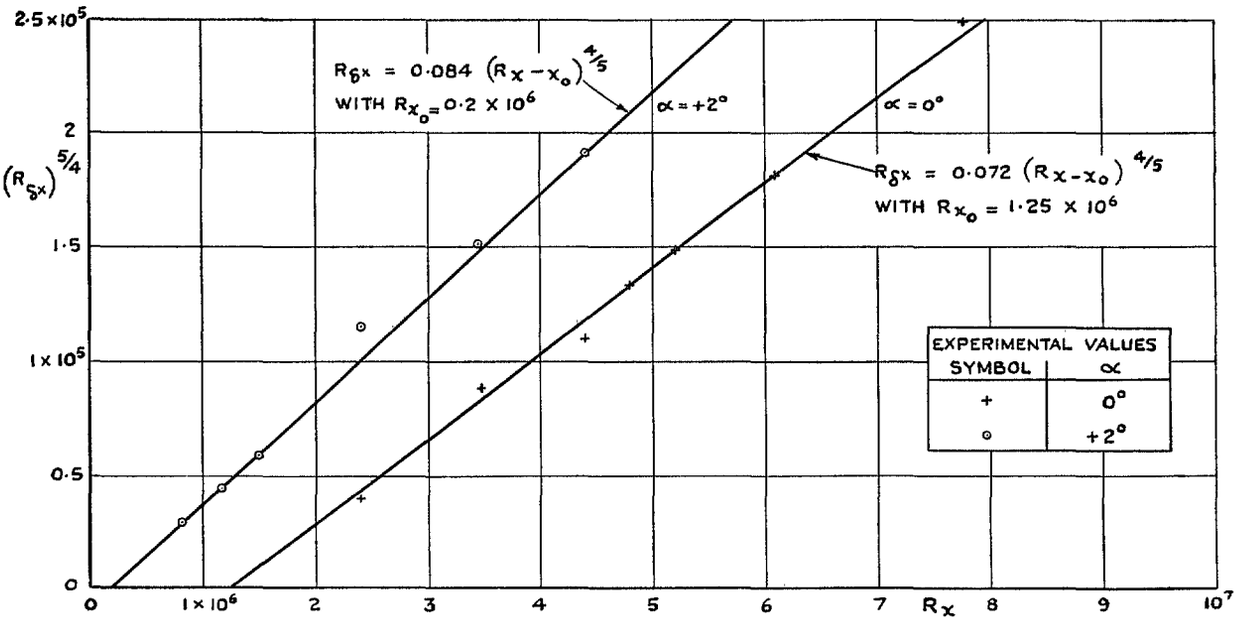

FIG. 13. Variation of displacement thickness of turbulent boundary layer on top generator of 15-deg cone with Reynolds number and incidence ($M_\infty = 3 \cdot 17$).

(76074) Wt. 53/2293 K.7 2/60 Hw. PRINTED IN ENGLAND

Publications of the Aeronautical Research Council

ANNUAL TECHNICAL REPORTS OF THE AERONAUTICAL RESEARCH COUNCIL (BOUND VOLUMES)

1939 Vol. I. Aerodynamics General, Performance, Airscrews, Engines. 50*s.* (52*s.*).
Vol. II. Stability and Control, Flutter and Vibration, Instruments, Structures, Seaplanes, etc. 63*s.* (65*s.*)

1940 Aero and Hydrodynamics, Aerofoils, Airscrews, Engines, Flutter, Icing, Stability and Control, Structures, and a miscellaneous section. 50*s.* (52*s.*)

1941 Aero and Hydrodynamics, Aerofoils, Airscrews, Engines, Flutter, Stability and Control, Structures. 63*s.* (65*s.*)

1942 Vol. I. Aero and Hydrodynamics, Aerofoils, Airscrews, Engines. 75*s.* (77*s.*)
Vol. II. Noise, Parachutes, Stability and Control, Structures, Vibration, Wind Tunnels. 47*s.* 6*d.* (49*s.* 6*d.*)

1943 Vol. I. Aerodynamics, Aerofoils, Airscrews. 80*s.* (82*s.*)
Vol. II. Engines, Flutter, Materials, Parachutes, Performance, Stability and Control, Structures. 90*s.* (92*s.* 9*d.*)

1944 Vol. I. Aero and Hydrodynamics, Aerofoils, Aircraft, Airscrews, Controls. 84*s.* (86*s.* 6*d.*)
Vol. II. Flutter and Vibration, Materials, Miscellaneous, Navigation, Parachutes, Performance, Plates and Panels, Stability, Structures, Test Equipment, Wind Tunnels. 84*s.* (86*s.* 6*d.*)

1945 Vol. I. Aero and Hydrodynamics, Aerofoils. 130*s.* (132*s.* 9*d.*)
Vol. II. Aircraft, Airscrews, Controls. 130*s.* (132*s.* 9*d.*)
Vol. III. Flutter and Vibration, Instruments, Miscellaneous, Parachutes, Plates and Panels, Propulsion. 130*s.* (132*s.* 6*d.*)
Vol. IV. Stability, Structures, Wind Tunnels, Wind Tunnel Technique. 130*s.* (132*s.* 6*d.*)

Annual Reports of the Aeronautical Research Council—
1937 2*s.* (2*s.* 2*d.*) 1938 1*s.* 6*d.* (1*s.* 8*d.*) 1939–48 3*s.* (3*s.* 5*d.*)

Index to all Reports and Memoranda published in the Annual Technical Reports, and separately—
April, 1950 - - - - R. & M. 2600 2*s.* 6*d.* (2*s.* 10*d.*)

Author Index to all Reports and Memoranda of the Aeronautical Research Council—
1909—January, 1954 R. & M. No. 2570 15*s.* (15*s.* 8*d.*)

Indexes to the Technical Reports of the Aeronautical Research Council—

December 1, 1936—June 30, 1939	R. & M. No. 1850	1*s.* 3*d.* (1*s.* 5*d.*)
July 1, 1939—June 30, 1945	R. & M. No. 1950	1*s.* (1*s.* 2*d.*)
July 1, 1945—June 30, 1946	R. & M. No. 2050	1*s.* (1*s.* 2*d.*)
July 1, 1946—December 31, 1946	R. & M. No. 2150	1*s.* 3*d.* (1*s.* 5*d.*)
January 1, 1947—June 30, 1947	R. & M. No. 2250	1*s.* 3*d.* (1*s.* 5*d.*)

Published Reports and Memoranda of the Aeronautical Research Council—

Between Nos. 2251–2349	R. & M. No. 2350	1*s.* 9*d.* (1*s.* 11*d.*)
Between Nos. 2351–2449	R. & M. No. 2450	2*s.* (2*s.* 2*d.*)
Between Nos. 2451–2549	R. & M. No. 2550	2*s.* 6*d.* (2*s.* 10*d.*)
Between Nos. 2551–2649	R. & M. No. 2650	2*s.* 6*d.* (2*s.* 10*d.*)
Between Nos. 2651–2749	R. & M. No. 2750	2*s.* 6*d.* (2*s.* 10*d.*)

Prices in brackets include postage

HER MAJESTY'S STATIONERY OFFICE

York House, Kingsway, London W.C.2; 423 Oxford Street, London W.1; 13a Castle Street, Edinburgh 2; 39 King Street, Manchester 2; 2 Edmund Street, Birmingham 3; 109 St. Mary Street, Cardiff; Tower Lane, Bristol 1; 80 Chichester Street, Belfast, *or through any bookseller.*

S.O. Code No. 23-3133